Tribol Lett (2014) 55:363–369
DOI 10.1007/s11249-014-0360-x

ORIGINAL PAPER

Temperature Dependences in the Tomlinson/Prandtl Model for Atomic Sliding Friction

Sergio J. Manzi · Wilfred T. Tysoe · Octavio J. Furlong

Received: 29 March 2014 / Accepted: 10 June 2014 / Published online: 28 June 2014
© Springer Science+Business Media New York 2014

Abstract The temperature dependence of the Tomlinson/Prandtl model for nanoscale sliding friction is analyzed by considering the properties of the initial and final states between which the tip can move, as well as the energy barrier between them, for various sliding regimes defined by the value of the corrugation factor γ. When $\gamma < 1$, the friction force tends to zero, defining a so-called superlubricious regime. The most commonly observed behavior is found for $\gamma > 4.603$, where the friction force increases monotonically with increasing sliding velocity up to a critical value equal to the value of F^* (lateral force at $T = 0$) and monotonically decreases with temperature from F^* at $T = 0$. However, completely different behavior is found when $1 < \gamma < 4.603$. The temperature dependence of the lateral force in this regime is investigated using Monte Carlo simulations. The friction force still tends to F^* as T approaches 0 K, but in contrast to the behavior found when $\gamma > 4.603$, the friction force increases with increasing temperature from F^*, reaches a maximum value, and then decreases monotonically as the temperature rises further. Such behavior has been observed in atomic force microscopy friction measurements.

Keywords Tomlinson/Prandtl model · Monte Carlo simulations · Periodic sliding potentials · Temperature dependence

S. J. Manzi · O. J. Furlong (✉)
INFAP/CONICET, Universidad Nacional de San Luis, Ejército de los Andes 950, 5700 San Luis, Argentina
e-mail: ojfurlong@unsl.edu.ar; ojfurlong@gmail.com

W. T. Tysoe
Department of Chemistry and Laboratory for Surface Studies, University of Wisconsin-Milwaukee, Milwaukee, WI 53211, USA

1 Introduction

The atomistic Tomlinson/Prandtl model [1, 2] has been successfully used to describe the velocity and temperature dependences of friction forces in nanoscale sliding, measured by means of atomic force microscopy (AFM) [3–5]. The Tomlinson/Prandtl model makes use of a simple sinusoidal sliding potential to mimic the tip-surface energy corrugation and a superimposed, moving harmonic potential to represent the elastic cantilever. The effect of the motion of the cantilever on the shape of the potential is illustrated in Fig. 1a, which results in a time-dependent evolution of the combined harmonic + sinusoidal surface potential. Here, the height of the sinusoidal surface potential is $E_0 = 0.317$ eV, the lattice periodicity $a = 0.29$ nm, and the cantilever force constant k_L is 0.6 N/m, values that are typical of AFM friction measurements. The tip is initially trapped in a potential minimum as illustrated by the vertical dotted lines on Fig. 1a, b. At temperature $T = 0$ K, spontaneous sliding occurs when an inflection point appears in the combined harmonic + sinusoidal potential, resulting in a transition to the next minimum in the potential, as illustrated in the top curves of Fig. 1a, b. This results in stick–slip motion. At a finite temperature $T > 0$, velocity and temperature dependences are incorporated into the model by assuming that thermally activated transitions of the tip can occur before the energy barrier ΔE has decreased to zero (when the height of the combined harmonic + sinusoidal potential is $\sim k_B T$, where k_B is the Boltzmann constant [6]). Thus, spontaneous sliding occurs when the inflection point appears ($\Delta E = 0$), at a lateral force defined as F^*, and thermally activated sliding at higher temperatures generally leads to values of friction lower than F^*.

The thermally activated Tomlinson/Prandtl model cannot be solved analytically; however, semi-analytical

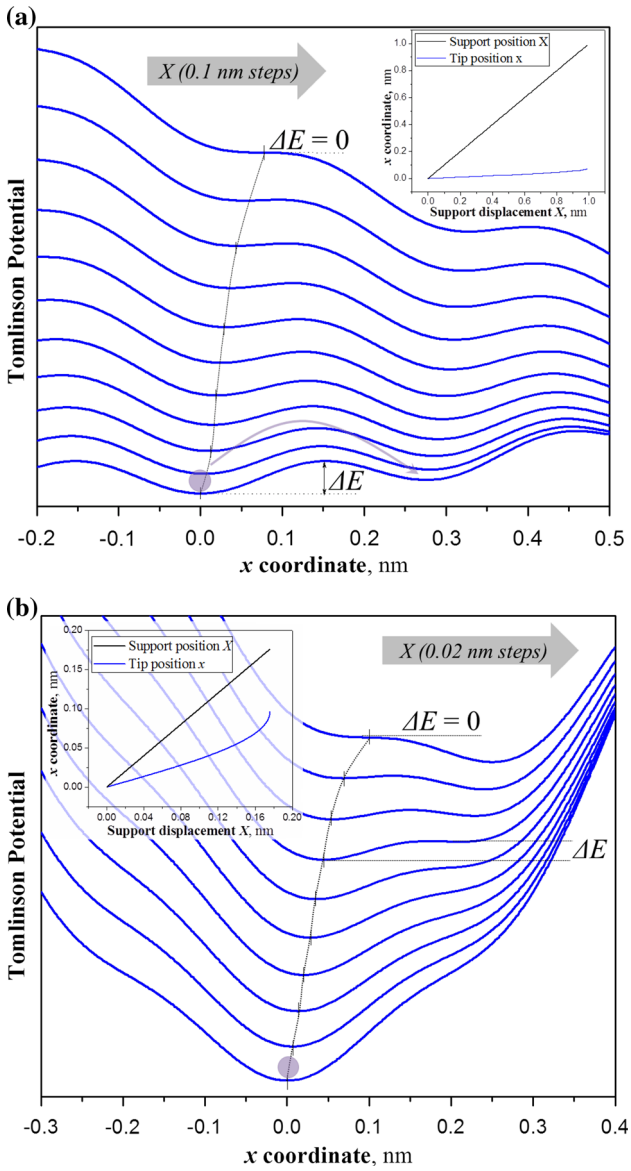

Fig. 1 Schematic illustration of the evolution of the shapes of the combined sinusoidal + harmonic surface potential in the Tomlinson/Prandtl model as the cantilever moves across the surface, as a function of the cantilever position using $E_0 = 0.317$ eV and $a = 0.29$ nm. Plot **a** shows the shapes of the potentials for a cantilever force constant $k_L = 0.6$ N/m yielding $\gamma = 19.868$, with each curve corresponding to changes in the support position X of 0.1 nm starting from zero. Plot **b** shows the evolution of the shapes of the potentials for a cantilever force constant $k_L = 6.0$ N/m yielding $\gamma = 1.987$, with each curve corresponding to a change in X of 0.02 nm starting from zero. Marked also as *vertical dotted lines* are the positions of the initial minima in the potential, which are shown plotted as function of cantilever position in the *insets*

solutions [7] have been obtained for the velocity and temperature dependences of the friction force, by approximating the variation in ΔE with the lateral force F_L as $\Delta E(F^* - F_L)^{3/2}$ [8]. In addition, it is assumed that all of the energy is dissipated as the tip moves (slips) from one stable position to the next. The semi-analytical solution predicts a monotonic increase in friction force with increasing velocity up to a maximum value equal to the value of F^*; and a monotonic decrease with increasing temperature, from an initial value of F^* at $T = 0$. The solution, in particular of the velocity dependence, has been confirmed experimentally [6, 7, 9, 10]. However, recent nanoscale friction experiments have revealed temperature dependences that do not agree with the predictions of this commonly used, semi-analytical solution. Specifically, a plateau or a maximum in the friction force is found at low temperatures [11–14], after which the friction force decreases with increasing temperature.

In view of the failure of the semi-analytical solutions of the Tomlinson/Prandtl model to predict this behavior, other effects, such as athermal instabilities induced by instrument noise [15], or the existence of two competing activated processes involving the formation and rupture of an ensemble of atomic contacts [14], have been invoked. The following demonstrates that such temperature dependences can still be successfully modeled within the context of the classical Tomlinson/Prandtl model, by properly considering the dynamics of all the critical points involved in the transition: the stable point at which the tip is trapped before the transition, the energy barrier that the tip needs to overcome, and the final stable position to which the tip moves. These effects are generally not completely included in the semi-analytical solution, which considers only the initial state of the transition, and implicitly assumes that there is always a final stable state to which the tip can move.

2 Results

Figure 1a shows the evolution of the Tomlinson/Prandtl potentials as a function of the support positions X, plotted in increments of 0.1 nm, starting from $X = 0$. Here, $E_0 = 0.317$ eV, the lattice periodicity $a = 0.29$ nm, and the cantilever force constant k_L is 0.6 N/m. The potentials clearly show the presence of an initial minimum (stable tip position), an activation energy barrier for the transition of height ΔE, and a final state into which the tip can move (neighboring stable position), for all possible support positions. The effect of increasing the cantilever force constant k_L to 6 N/m while keeping the other parameters constant is shown in Fig. 1b for different support positions X, displayed in increments of 0.02 nm starting from $X = 0$. Now, the much sharper parabola arising from larger k_L values initially results in the absence of a neighboring minimum in the potential energy curve, resulting in the absence of a stable position to accommodate the tip after sliding. However, additional motion of the cantilever

eventually induces the appearance of a neighboring minimum, in this case for a cantilever displacement of ~0.114 nm. Further increasing the cantilever force constant eventually results in harmonic + sinusoidal potential energy curves in which a neighboring minimum never appears regardless of the support position, so that no energy can be dissipated during sliding, resulting in so-called superlubricity [16]. This suggests that there are three distinct friction regimes for different values of E_0, k_L, and a. It has been shown that different friction regimes can be defined based on the so-called corrugation factor γ [17, 18], which is the ratio between the strength of the tip-sample interaction and the elastic energy of the system, and can be expressed as:

$$\gamma = \frac{2\pi^2 E_0}{k_L a^2}. \quad (1)$$

It is well known that for $\gamma \leq 1$, the model predicts the superlubricious or ultra-low friction regime, where friction tends to zero since the instabilities that, under stick–slip conditions give rise to the dominant energy dissipation mechanism, disappear [16].

In order to determine the limiting values of γ that define the other regimes, it is necessary to define the conditions for the appearance of all critical points (minima, maxima, and inflection points) in the Tomlinson–Prandtl potential $V(x,t)$:

$$V(x,t) = -\frac{E_0}{2}\cos\left(\frac{2\pi x}{a}\right) + \frac{k_L}{2}(vt - x)^2, \quad (2)$$

where v is the scanning velocity, so that vt becomes the time-dependent position of the tip support, X (Fig. 1). Critical points are given by $\partial V/\partial x = 0$. Thus, at a tip support position $X = 0$, the positions of the critical points x_C can be expressed as:

$$k_L x_C = -\frac{\pi E_0}{a}\sin\left(\frac{2\pi x_C}{a}\right). \quad (3)$$

Similar analyses have been performed previously to account for the energy dissipation during tip transitions [19]. The right-hand side of Eq. 3 is represented in Fig. 2 by the solid (sinusoidal) curve, while the solid straight lines plot $k_L x$ for different values of k_L, where typical experimental parameters, $E_0 = 0.317$ eV, $a = 0.29$ nm, and $k_L = 0.6$, 2.59 and 6.0 N/m, have been chosen [10]. When Eq. (3) is satisfied, stable critical points occur when the straight lines (representing $k_L x$) intercept the sinusoid. For large γ values, for example when $k_L = 0.6$ N/m ($\gamma = 19.87$, solid line with square), there are multiple solutions, and both forward and backward transitions are allowed, and multiple jumps [17] may occur, even when the tip is fully relaxed ($x = 0$, $X = 0$; therefore, $F_L = 0$). In such cases, there is always a final state to which the tip

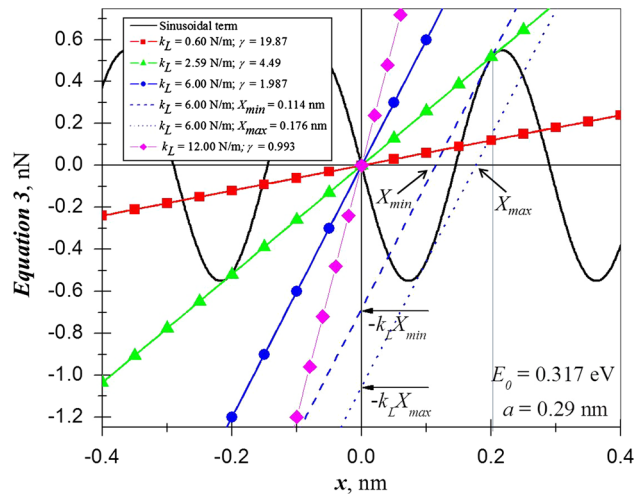

Fig. 2 Graphic representation of Eq. (3). The right-hand side of Eq. (3) is represented by the *solid* (sinusoidal) *curve*, while the *solid dotted straight lines* represent $k_L x$ for different values of k_L, using $E_0 = 0.317$ eV and $a = 0.29$ nm. The y intercept of the *dashed straight line* represents the minimum support displacement required to induce the appearance of a neighboring stable position, and the y intercept of the *dotted straight line* indicates the support displacement at which ΔE becomes zero

can move, and the semi-analytical solutions to the Tomlinson/Prandtl model apply at relatively low temperatures and/or relatively high speeds, where the occurrence of backward jumps can be neglected.

At the other extreme, for $\gamma < 1$, for example when $k_L = 12.0$ N/m ($\gamma = 0.993$, solid line with diamond), no transitions are allowed since there is never a neighboring stable position into which the tip can move regardless of the value of F_L. In other words, there are no solutions for which $\partial^2 V/\partial x^2 < 0$; no energy is dissipated during sliding, giving rise to so-called superlubricity [16].

In the intermediate regime, for example, when $k_L = 6.0$ N/m ($\gamma = 1.987$, solid line with circle), there are no stable positions into which to move from $x = 0$ when $F_L = 0$. However, in this case, a stable final state is created as sliding occurs. This is illustrated in Fig. 2 where the support has to be displaced a minimum distance $X_{min} \sim 0.114$ nm (indicated by the arrow, corresponding to $F_{Lmin} = k_L(X_{min} - x) = 0.433$ nN, to allow the straight line (solid line with circle) to intercept the sinusoid and create a neighboring stable position in the displacement direction (dashed straight line, Fig. 2). Also shown in Fig. 2 (for $k_L = 6.0$ N/m) is the *maximum* support displacement ($X_{max} = 0.176$ nm, dotted line, Fig. 2) for which the energy barrier decreases to zero ($\Delta E = 0$ and $F_L = F^*$), and the tip jumps regardless of the values of temperature. The condition for the transition to this regime is illustrated by the line for $k_L = 2.59$ N/m (solid line with triangle), where only one possible solution remains for

each direction at $X = 0$, such that transitions to neighboring stable points only occur for $k_L \geq 2.59$ N/m, for which the usual semi-analytical solution can be considered. The value of γ for the transition between these regimes can be determined by equating the first derivative of both sides of Eq. (3), since it is the only solution for which the slopes of the two terms in this equation have the same values with respect to the coordinate x in the potential (Fig. 2). This defines the position ζ for the appearance of a point of inflection in the potential for $X = 0$ and is given by

$$\frac{2\pi\zeta}{a} = \tan\left(\frac{2\pi\zeta}{a}\right) = 4.4934\ldots \tag{4}$$

Using $a = 0.29$ nm, $\zeta = 0.2074$ nm, corresponding to the displacement shown as a vertical line in Fig. 2. Equation (3) is valid for all critical points. Substituting ζ for x_C with $E_0 = 0.317$ eV gives a value of $k_L = 2.59$ N/m (solid line with triangle); substituting these values into Eq. (1) yields a limiting value of $\gamma = 4.603$, in agreement with the previous results [18].

Thus, three distinct friction regimes can be defined depending on the value of γ. For $\gamma \leq 1$, no final states exist to which the tip can move, regardless of the support displacement; the friction force tends to zero, producing so-called superlubricity [16]. A second regime is defined for $1 < \gamma < 4.603$, where a final stable state is induced by sliding; while in the third regime, for $\gamma \geq 4.603$, there are always stable final states into which the tip can jump.

Because of the need to consider the creation of final states in the intermediate regime ($1 < \gamma < 4.603$), it is not generally possible to develop semi-analytical models as could be done for $\gamma > 4.603$, although recently analytical models that include final state effects have been developed for the limiting cases of $\gamma \to 1$ and $\gamma \gg 1$ [18]. However, no direct relations to the temperature dependences of the lateral force were made. In order to obtain general solutions, Monte Carlo simulations of the one-dimensional classical Tomlinson model were performed for this intermediate regime. This strategy has previously been used to explore velocity effects on sliding friction, and it has been demonstrated that it precisely reproduces the solution of the sinusoidal Tomlinson/Prandtl model [20, 21]. The Monte Carlo simulations use a thermally activated transition rate w over the time-dependent energy barrier $\Delta E(t)$ described by

$$w(t) = f_0 \exp\left[-\frac{\Delta E(t)}{k_B T}\right], \tag{5}$$

where f_0 is the attempt frequency of a transition. For each Monte Carlo trial, the value of w is calculated at some time t and compared to a random number ξ uniformly distributed in the interval (0,1). If $\xi < w$, the transition occurs, where both backward and forward motions are allowed. The resulting transition lateral force is recorded as a function of time. The process is repeated a sufficient number of times to yield an average friction force (F_L) with negligible statistical error. The conversion between Monte Carlo and real time is made by defining an elementary transition probability per unit time [22]. Prior to the simulations, the position and energy of the critical points (maxima and minima) of the combined sinusoidal + harmonic potential are calculated as a function of the cantilever displacement and stored in a position matrix. This is then used as an input file to avoid having to define them for each trial.

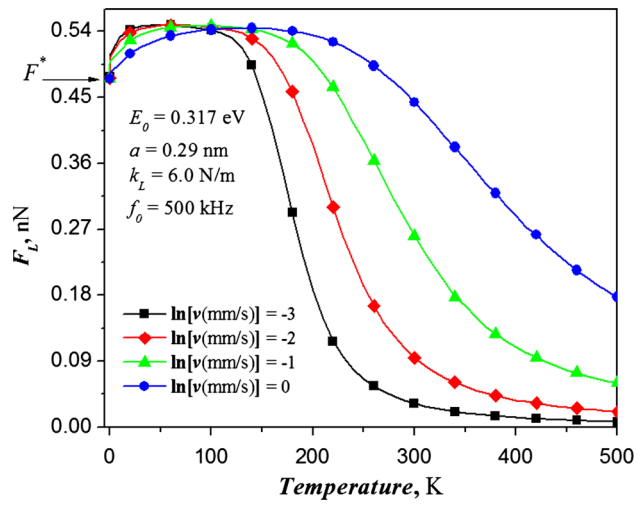

Fig. 3 Simulated results of lateral force (F_L) with temperature, T, for different values of velocity ($\ln(v)$), using $f_0 = 500$ kHz, $E_0 = 0.317$ eV, $a = 0.29$ nm, and $k_L = 6.0$ N/m. Indicated on the y-axis is the corresponding value of F^*

Figure 3 displays the simulated results of lateral force versus temperature at different velocities in the intermediate regime ($\gamma = 1.987$) with $k_L = 6.0$ N/m using $f_0 = 500$ kHz, typical of AFM experiments [4, 7], with the remainder of the parameters being identical to those used in Fig. 2. The lateral force at $T = 0$ K corresponds to F^*, where according to the semi-analytical model, a monotonic decrease to zero with increasing temperature should be observed [7]. However, for $\gamma = 1.987$, the simulation shows an initial increase in lateral force with temperature from F^* up to a maximum value, from which it then decreases monotonically with temperature. Similar experimental variations in friction force with temperature have been found, showing an increase to a maximum value or a friction plateau, and a subsequent decrease with temperature [11–14].

3 Discussion

Three distinct friction regimes have been defined: a superlubricious regime for $\gamma \leq 1$; an intermediate regime for

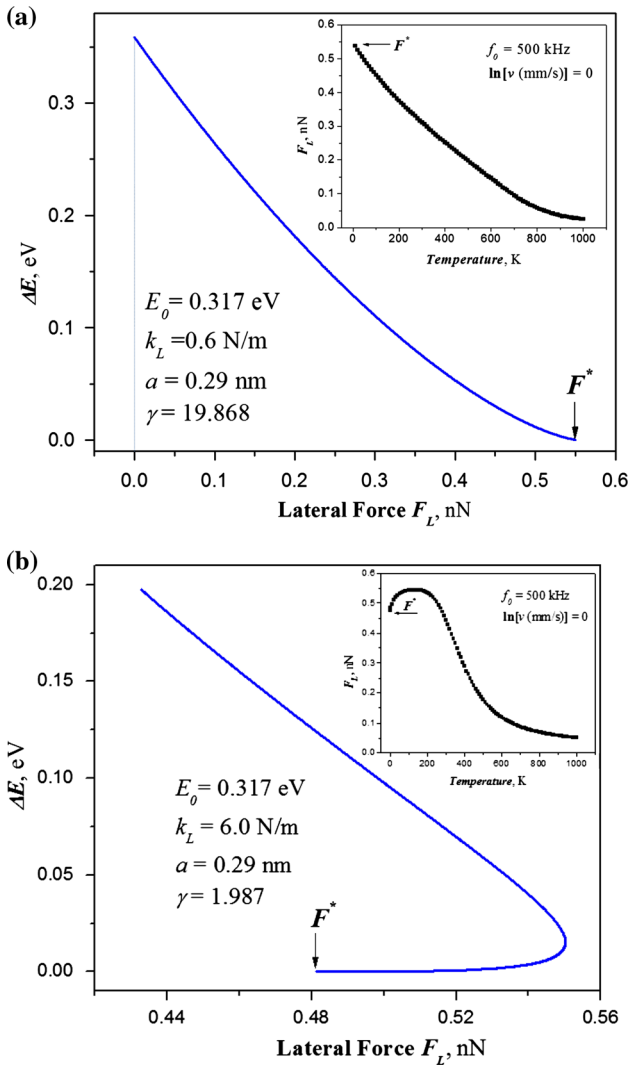

Fig. 4 Plots of the height of the barrier ΔE versus lateral force F_L using $E_0 = 0.317$ eV and $a = 0.29$ nm. Plot **a** shows the behavior for a cantilever force constant $k_L = 0.6$ N/m yielding $\gamma = 19.868$, and plot **b** shows the behavior for a cantilever force constant $k_L = 6.0$ N/m yielding $\gamma = 1.987$. Shown as *insets* are the resulting variations in sliding force with temperature

$1 < \gamma < 4.603$, producing unusual temperature dependences; and a third regime for $\gamma \geq 4.603$ for which the semi-analytical model can be applied.

The anomalous temperature dependence of the friction force identified in the intermediate regime depends on two effects. The first is the absence of a neighboring minimum into which the tip can move, which only appears after the cantilever has been displaced a certain distance. This contrasts the behavior for $\gamma > 4.603$, where a neighboring minimum is always present (Fig. 1a). This behavior is illustrated in Fig. 4a. When the cantilever is at $X = 0$ (lateral force = 0), the barrier height is at its maximum. As the cantilever moves, the barrier height decreases, reaching a value of zero (to produce and inflection point) at a lateral force equal to F^*. The shape of this curve can be reasonably approximated by $\Delta E\ (F^* - F_L)^{3/2}$ as used for the semi-analytical solutions [8], giving rise to the monotonic decrease in friction force with increasing temperature, shown as an inset in Fig. 4a. In addition, the tip positions in the initial potential minima vary only slightly compared to the displacement of the cantilever, as emphasized by the inset to Fig. 1a. Note that, in this regime, the maximum lateral force is equal to the value of F^*.

This behavior is compared with that for the change in energy barrier as a function of lateral force for the intermediate regime ($k_L = 6.0$ N/m, $\gamma = 1.987$) in Fig. 4b. In this case, since no stable final state appears until a minimum lateral force (of 0.44 nN) has been applied, only values of the energy barrier for lateral forces above this value have any physical meaning. The shape of the curve for larger values of lateral displacement is now completely different from that shown in Fig. 4a. The value of ΔE decreases monotonically as the cantilever moves, up to a maximum value of the lateral force greater than F^*. After this point, as ΔE approaches zero, lower values of the lateral force are found down to F^* at $\Delta E = 0$. Thus, while F^* represents the maximum lateral force than can be obtained in the regime where $\gamma > 4.603$, larger lateral forces than this value can be obtained in the intermediate regime. Thus, in addition to some additional lateral force being required for an adjacent minimum to appear in the sliding potential, there is a second effect that is responsible for the behavior of ΔE versus lateral force seen in Fig. 4b. The origin of this effect can be observed in Fig. 1b. Here, the initial position of the tip moves more slowly compared to the support prior to the appearance of an adjacent stable state. However, once the final state appears, there is a larger change in the initial position of the tip compared to the support displacement, due to the influence of the sharper harmonic potential as a consequence of the larger cantilever force constant. This results in the tip moving more rapidly than the cantilever as ΔE tends to zero, decreasing $(X - x)$, thereby causing the lateral force to decrease to F^* when the inflection point appears, producing the behavior illustrated in Fig. 4b. The temperature dependence observed in the simulations (Fig. 3) arises since higher temperatures lead to transitions occurring for values of ΔE larger than zero (of the order of $k_B T$). Thus, at $T = 0$, sliding can only occur when an inflection point appears (at F^*). As the temperature increases, states with larger values of ΔE can be probed, causing an initial increase in the lateral force (Fig. 4b). However, as $k_B T$ exceeds the energy at which the maximum force appears (Fig. 4b), the behavior becomes analogous to that found in Fig. 4a, where ΔE decreases monotonically with

lateral force, so that the friction force then decreases with increasing temperature. The resulting temperature dependence is that shown in Fig. 3 and the inset in Fig. 4b.

It is important to note that these regimes (based on the parameter γ) have been analyzed using a classical sinusoidal surface potential. However, it has been shown that the surface potentials are more realistically represented by non-sinusoidal surface potentials [21]. Thus, by definition, the expression for γ, and consequently the range of γ values that determine the different frictional regimes, will clearly depend on the shape of the surface potentials. Thus, while the simple sinusoidal potential used in this work qualitatively reproduces the unusual temperatures dependences found experimentally [11–14] without having to invoke noise effects [15] or multiple activation steps [13], quantitatively reproducing the experimental data will require the use of more realistic potentials.

4 Conclusions

By properly applying the classical one-dimensional Tomlinson/Prandtl model, and only considering a single thermally activated transition, it is possible to qualitatively reproduce all experimentally observed temperature dependences of the friction force in AFM experiments. By a detailed consideration of the existence or creation of final states during sliding, three friction regimes are defined depending on the value of the corrugation factor γ, in agreement with the previous results [18]. Here, the temperature dependence of the lateral force within these regimes is explained. First, it is the previously identified superlubricious regime, which occurs for $\gamma \leq 1$. In the second regime, for $1 < \gamma < 4.603$, a final stable state is induced by sliding where a rapid variation in tip position as ΔE approaches zero leads to maxima in the plot of friction force versus temperature. The third regime, with $\gamma \geq 4.603$, yields a friction force that varies monotonically with temperature for which the semi-analytical solutions can be applied. In addition, the limitations of applying the commonly used semi-analytical solution to interpret experimental data are highlighted, since the semi-analytical solution assumes that $\Delta E \propto (F^* - F_{\mathrm{L}})^{3/2}$. However, as γ approaches the limiting value of 4.603, this approximation becomes less valid.

While zero friction is obtained in the superlubricious regime, it is demonstrated that Monte Carlo methods can provide solutions to the Tomlinson/Prandtl model in the second regime (where $1 < \gamma < 4.603$), without having to invoke any other effects or assumptions external to the model.

Acknowledgments We gratefully acknowledge the National Science Foundation under Grant Number CMMI 0826151, the CONICET (Argentina) for support of this work, and Prof. Victor Pereyra for helpful discussions.

References

1. Tomlinson, G.A.: A molecular theory of friction. Philos. Mag. **7**, 905–937 (1929)
2. Prandtl, L.: Ein Gedankenmodell zur kinetischen Theorie der festen Körper. Z. Angew. Math. Mech. **8**, 85 (1928)
3. Gnecco, E., Bennewitz, R., Gyalog, T., Meyer, E.: Friction experiments on the nanometre scale. J. Phys. Condens. Matter **13**, R619–R642 (2001)
4. Szlufarska, I., Chandross, M., Carpick, R.W.: Recent advances in single-asperity nanotribology. J. Phys. D Appl. Phys. **41**, 123001 (2008)
5. Dong, Y., Vadakkepatt, A., Martini, A.: Analytical models for atomic friction. Tribol. Lett. **44**, 367–386 (2011)
6. Gnecco, E., Bennewitz, R., Gyalog, T., Loppacher, C., Bammerlin, M., Meyer, E., Güntherodt, H.H.: Velocity dependence of atomic friction. Phys. Rev. Lett. **84**, 1172–1175 (2000)
7. Riedo, E., Gnecco, E., Bennewitz, R., Meyer, E., Brune, H.: Interaction potential and hopping dynamics governing sliding friction. Phys. Rev. Lett. **91**, 084502 (2003)
8. Sang, Y., Dubé, M., Grant, M.: Thermal effects on atomic friction. Phys. Rev. Lett. **87**, 174301 (2001)
9. Jansen, L., Hölscher, H., Fuchs, H., Schirmeisen, A.: Temperature dependence of atomic-scale stick–slip friction. Phys. Rev. Lett. **104**, 256101 (2010)
10. Li, Q., Dong, Y., Perez, D., Martini, A., Carpick, R.W.: Speed dependence of atomic stick–slip friction in optimally matched experiments and molecular dynamics simulations. Phys. Rev. Lett. **106**, 126101 (2011)
11. Zhao, X., Phillpot, S.R., Sawyer, W.G., Sinnott, S.B., Perry, S.S.: Transition from thermal to athermal friction under cryogenic conditions. Phys. Rev. Lett. **102**, 186102 (2009)
12. Greiner, C., Felts, J.R., Dai, Z., King, W.P., Carpick, R.W.: Controlling nanoscale friction through the competition between capillary adsorption and thermally-activated sliding. ACS Nano **6**, 4305–4313 (2012)
13. Barel, I., Urbakh, M., Jansen, L., Schirmeisen, A.: Unexpected temperature and velocity dependencies of atomic-scale stick–slip friction. Phys. Rev. B **84**, 115417 (2011)
14. Barel, I., Urbakh, M., Jansen, L., Schirmeisen, A.: Multibond dynamics of nanoscale friction: the role of temperature. Phys. Rev. Lett. **104**, 066104 (2010)
15. Dong, Y., Gao, H., Martini, A.: Suppression of atomic friction under cryogenic conditions: the role of athermal instability in AFM measurements. EPL **98**, 16002 (2012)
16. Socoliuc, A., Bennewitz, R., Gnecco, E., Meyer, E.: Transition from stick–slip to continuous sliding in atomic friction: entering a new regime of ultralow friction. Phys. Rev. Lett. **92**, 134301 (2004)
17. Medyanik, S.N., Liu, W.K., Sung, I., Carpick, R.W.: Predictions and observations of multiple slip modes in atomic-scale friction. Phys. Rev. Lett. **97**, 136106 (2006)
18. Gnecco, E., Roth, R., Baratoff, A.: Analytical expressions for the kinetic friction in the Prandtl–Tomlinson model. Phys. Rev. B **86**, 035443 (2012)
19. Müser, M.H.: Velocity dependence of kinetic friction in the Prandtl–Tomlinson model. Phys. Rev. B **84**, 125419 (2011)

20. Furlong, O.J., Manzi, S.J., Pereyra, V.D., Bustos, V., Tysoe, W.T.: Kinetic Monte Carlo theory of sliding friction. Phys. Rev. B **80**, 153408 (2009)
21. Furlong, O.J., Manzi, S.J., Pereyra, V.D., Bustos, V., Tysoe, W.T.: Monte Carlo simulations for Tomlinson sliding models for non-sinusoidal periodic potentials. Tribol. Lett. **39**, 177–180 (2010)
22. Sales, J.L., Uñac, R.O., Gargiulo, M.V., Bustos, V., Zgrablich, G.: Monte Carlo simulation of temperature programmed desorption spectra: a guide through the forest for monomolecular adsorption on a square lattice. Langmuir **12**, 95–100 (1996)